

Determination of sprite streamers altitude based on N 2 spectroscopic analysis

Mohand A. Ihaddadene, Sébastien Celestin

▶ **To cite this version:**

Mohand A. Ihaddadene, Sébastien Celestin. Determination of sprite streamers altitude based on N 2 spectroscopic analysis. Journal of Geophysical Research Space Physics, 2017, 122 (1), pp.1000 - 1014. 10.1002/2016JA023111 . insu-01503097

HAL Id: insu-01503097
https://insu.hal.science/insu-01503097

Submitted on 6 Apr 2017

HAL is a multi-disciplinary open access archive for the deposit and dissemination of scientific research documents, whether they are published or not. The documents may come from teaching and research institutions in France or abroad, or from public or private research centers.

L'archive ouverte pluridisciplinaire **HAL**, est destinée au dépôt et à la diffusion de documents scientifiques de niveau recherche, publiés ou non, émanant des établissements d'enseignement et de recherche français ou étrangers, des laboratoires publics ou privés.

AGU PUBLICATIONS

JGR

Journal of Geophysical Research: Space Physics

RESEARCH ARTICLE
10.1002/2016JA023111

Key Points:
- Development of a simulation-based method to estimate the altitude of streamers in TLEs from spectrophotometric measurements
- Determination of streamer velocity and peak electric field
- Improve the scientific return of space missions devoted to the study of TLEs from a nadir-viewing geometry

Correspondence to:
M. A. Ihaddadene,
mohand.ihaddadene@cnrs-orleans.fr

Citation:
Ihaddadene, M. A., and S. Celestin (2017), Determination of sprite streamers altitude based on N_2 spectroscopic analysis, *J. Geophys. Res. Space Physics*, *122*, 1000–1014, doi:10.1002/2016JA023111.

Received 24 JUN 2016
Accepted 5 DEC 2016
Accepted article online 10 DEC 2016
Published online 18 JAN 2017

©2016. American Geophysical Union. All Rights Reserved.

Determination of sprite streamers altitude based on N_2 spectroscopic analysis

Mohand A. Ihaddadene[1] **and Sebastien Celestin**[1]

[1] LPC2E, University of Orleans, CNRS, Orleans, France

Abstract Future space missions (e.g., ASIM and TARANIS) are soon to be launched to observe transient luminous events (TLEs) from a nadir-viewing geometry. The mission GLIMS already performed observations of TLEs from a nadir-viewing geometry on board the International Space Station. Although this observation geometry is of first interest to study TLEs, it makes the determination of some quantities, such as streamer altitudes, very difficult. In this study, we propose a method to estimate the altitude of downward propagating sprite streamers using a spectrophotometric approach. Using a plasma fluid model, we simulate sprite streamers at different altitudes and quantify their optical emissions in the Lyman-Birge-Hopfield (LBH) (~100–260 nm), the first positive ($1PN_2$) (~650–1070 nm), and the second positive ($2PN_2$) (~330–450 nm) bands systems of molecular nitrogen and the first negative ($1NN_2^+$) (~390–430 nm) bands systems of N_2^+. The estimation of associated ratios allows to trace back the electric field in the streamer head as well as the altitude at which the streamer is propagating owing to different dependencies of quenching processes on the air density. The method takes into account the nonsteady state of the populations of some excited species and the exponential expansion of the streamer. The reported results could potentially be used for all TLEs but is of special interest in the case of column sprites or at the early stage of carrot sprites.

1. Introduction

Sprites are large optical phenomena that last a few milliseconds and that are produced typically by positive cloud-to-ground (+CG) lightning between 40 and 90 km altitude [e.g., *Franz et al.*, 1990; *Winckler et al.*, 1993; *Pasko*, 2007; *Chen et al.*, 2008; *Stenbaek-Nielsen et al.*, 2013; *Pasko et al.*, 2013, and references therein]. Sprites belong to the wider family of transient luminous events (TLEs) [e.g., *Pasko et al.*, 2012]. Studies have showed that sprites are composed of filamentary plasma structures called streamer discharges [e.g., *Pasko et al.*, 1998; *Gerken et al.*, 2000; *Stanley et al.*, 1999]. Some sprites can be highly complex and composed of many streamers [e.g., *Stanley et al.*, 1999; *Gerken et al.*, 2000; *Stenbaek-Nielsen et al.*, 2000], while some are composed of only a few filaments [e.g., *Wescott et al.*, 1998, *Wescott et al.*, 1998; *Adachi et al.*, 2004]. The different sprite morphologies are understood to be due to different upper atmospheric ambient conditions and the characteristics of the causative lightning discharge [e.g., *Qin et al.*, 2013a, 2013b, 2014, and references therein].

One of the ways used to explore the physical properties of sprites is the spectroscopic diagnostic of their optical emissions, specifically in the following bands systems of N_2: the Lyman-Birge-Hopfield (LBH) ($a^1\Pi_g \rightarrow X^1\Sigma_g^+$) [e.g., *Liu and Pasko*, 2005; *Liu et al.*, 2006; *N. Liu et al.*, 2009; *Gordillo-Vázquez et al.*, 2011], the first positive $1PN_2$ ($B^3\Pi_g \rightarrow A^3\Sigma_u^+$) [e.g., *Mende et al.*, 1995; *Hampton et al.*, 1996; *Green et al.*, 1996; *Morrill et al.*, 1998; *Milikh et al.*, 1998; *Bucsela et al.*, 2003; *Kanmae et al.*, 2007; *Siefring et al.*, 2010; *Gordillo-Vázquez*, 2010; *Gordillo-Vázquez et al.*, 2011, 2012], the second positive $2PN_2$ ($C^3\Pi_u \rightarrow B^3\Pi_g$) [e.g., *Armstrong et al.*, 1998; *Morrill et al.*, 1998; *Milikh et al.*, 1998; *Suszcynsky et al.*, 1998; *Heavner et al.*, 2010; *Gordillo-Vázquez*, 2010; *Gordillo-Vázquez et al.*, 2011, 2012], and the first negative bands systems of N_2^+ ($1NN_2^+$) ($B^2\Sigma_u^+ \rightarrow X^2\Sigma_g^+$) [e.g., *Armstrong et al.*, 1998; *Suszcynsky et al.*, 1998; *Kanmae et al.*, 2010a]. Several works have been realized to determine the electric fields involved in sprite streamers based on their produced optical emissions [e.g., *Morrill et al.*, 2002; *Kuo et al.*, 2005; *Adachi et al.*, 2006; *Kanmae et al.*, 2010b], and some have showed an acceptable agreement with simulations [*Liu et al.*, 2006]. However, theoretical studies have also showed the existence of correction factors to be taken into account for the determination of an accurate value of the peak electric field in streamer heads. The correction factors are due to both a spatial shift between the maximum in the electric field at the head of the streamer and the maximum in the production of excited species and the fact that

most photons are produced some distance away from the filament symmetry axis [*Celestin and Pasko*, 2010; *Bonaventura et al.*, 2011].

The experiment LSO (Lightning and Sprite Observations) developed by the French Atomic Energy Commission (CEA) with the participation of the French Space Agency (CNES) [*Blanc et al.*, 2004], the Japanese Aerospace Exploration Agency (JAXA) mission GLIMS (Global Lightning and sprIte MeasurementS) [*Sato et al.*, 2015], and the future European Space Agency (ESA) mission ASIM (Atmosphere-Space Interactions Monitor) [*Neubert*, 2009] are dedicated to the observation of TLEs from the International Space Station (ISS). The Lomonosov Moscow State University satellite Universitetsky-Tatiana-2 observed TLEs from a Sun-synchronous orbit at 820–850 km [*Garipov et al.*, 2013]. The future satellite mission TARANIS (Tool for the Analysis of RAdiation from lightNIng and Sprites), funded by CNES, will observe TLEs from a Sun-synchronous orbit at an altitude of ~700 km [*Lefeuvre et al.*, 2008]. All the above mentioned space missions have adopted strategies based on nadir observation of TLEs. Observation from a nadir-viewing geometry is indeed especially interesting as it reduces the distance between the observation point and the event and hence minimizes atmospheric absorption and maximizes the chance of observing TLEs and their associated phenomena, such as electromagnetic radiation or possible high-energy emissions. However, in this observation geometry, the vertical dimension is poorly resolved, and so are the speeds of sprite substructures.

In this work, we investigate a spectrophotometric method to trace back the altitude of streamers in sprites using optical emissions that will be detected by ASIM [*Neubert*, 2009] and TARANIS [*Lefeuvre et al.*, 2008] and that were detected by GLIMS [*Sato et al.*, 2015]. As mentioned above, the electric field in sprite streamer heads can be estimated through spectroscopic analysis of ratios of bands systems intensities produced by molecular nitrogen-excited electronic states. These excited states can deexcite either radiatively, hence giving rise to bands systems, or through collisions with other molecules in a process named quenching. The probability of the latter deexcitation channel depends on the local atmospheric density and therefore on the altitude. Using the fact that the excited species $N_2(a^1\Pi_g)$ (responsible for LBH) and $N_2(B^3\Pi_g)$ (responsible for $1PN_2$) quench under relatively low pressure, and therefore at high altitudes, while $N_2(C^3\Pi_u)$ (responsible for $2PN_2$) and $N_2^+(B^2\Sigma_u^+)$ (responsible for $1NN_2^+$) are quenched below relatively high pressure and therefore low altitudes, we show that, combining observations with streamer modeling results, it is possible to obtain information about the production altitude of the optical emission through ratios of bands systems.

In section 2, we present the sprite streamer and spectroscopic models used in the present paper, in section 3 we show our results on electric field and altitude determination of sprite streamers, and we discuss the implication of our results in section 4.

2. Model Formulation

2.1. Streamer Model

The streamer model we use in the present study is based on the drift-diffusion equations for charged species coupled with Poisson's equation [*Ihaddadene and Celestin*, 2015]. We use the local electric field approximation, and thus, the transport coefficients and the local energy of electrons are explicit functions of the electric field. Hence, in our model, determining the energy or the electric field is equivalent, and the link between these two quantities is given by the Einstein relation $k_B T_e = \frac{q_e D_e(E)}{\mu_e(E)}$, where k_B is the Boltzmann constant, T_e is the electron temperature, q_e is the electron charge, D_e and μ_e are, respectively, the diffusion coefficients and the mobility of electrons, and E is the local electric field. In order to simulate streamer propagation in weak electric field lower than the conventional breakdown field $E_k = 29 \times \frac{N}{N_0}$ kV/cm [e.g., *Morrow and Lowke*, 1997], defined by the equality of the ionization and the two-body dissociative attachment frequencies in air, where $N_0 = 2.688 \times 10^{25}$ m^{-3} is the air density at ground level and N is the local air density according to the U.S. Standard Atmosphere [*Committee on Extension to the Standard Atmosphere*, 1976], we use a sphere-to-plane electrode configuration [e.g., *Babaeva and Naidis*, 1996a, 1996b] to initiate the streamer. A sphere of a radius $R_{sph} = 10^{-3} \times \frac{N_0}{N}$ m is set to a potential $\phi_0 = 0$ and 4.8 kV and placed in a weak uniform electric field $E_0 = 28 \times \frac{N}{N_0}$ kV/cm and $E_0 = 12 \times \frac{N}{N_0}$ kV/cm, respectively, in order to obtain a maximum amplitude of the electric field of $3E_k$ at the surface of the sphere [e.g., *Liu et al.*, 2006; *N. Liu et al.*, 2009]. In this study, we consider $E_0 = 28 \times \frac{N}{N_0}$ kV/cm and $E_0 = 12 \times \frac{N}{N_0}$ kV/cm as reasonable upper and lower limits of ambient electric fields at which the observed streamers develop in the early stage of sprites. This is in general agreement with

Table 1. Einstein Coefficient A_k (s^{-1}), Quenching Coefficients $\alpha_{1,2}$ (cm^3/s), Lifetime τ_k (s) at Ground Level Air of Different Excited States of N_2 Molecule, and Quenching Altitudes h_Q (km)[a]

	$N_2\,(a^1\Pi_g)$	$N_2\,(B^3\Pi_g)$	$N_2\,(C^3\Pi_u)$	$N_2^+\,(B^2\Sigma_u^+)$
A_k	1.8×10^4	1.7×10^5	2×10^7	$1.4\times10^7\ s^{-1}$
α_1	10^{-11}	10^{-11}	10^{-11}	4.53×10^{-10}
α_2	10^{-10}	3×10^{-10}	3×10^{-10}	7.36×10^{-10}
τ_k	1.33×10^{-9}	5.47×10^{-10}	5.41×10^{-10}	7.29×10^{-11}
h_Q	77	67	31	48

[a]See section 2.2 for citations.

observation-based estimates of *Hu et al.* [2007], *Li et al.* [2008], *N. Y. Liu et al.* [2009], and *Qin et al.* [2012]. Note that streamers are capable of propagating in electric field as low as $E_0 = 5\times\frac{N}{N_0}$ kV/cm [e.g., *Qin and Pasko*, 2014, and references therein].

Downward propagating positive streamers are initiated by placing a Gaussian of neutral plasma with characteristic sizes $\sigma_z = 10^{-4}\times\frac{N_0}{N}$ m, $\sigma_r = 10^{-4}\times\frac{N_0}{N}$ m, and $n_{e_0} = 10^{18}\times\frac{N^2}{N_0^2}$ m^{-3} in the vicinity of the sphere electrode. For more information about the scaling of physical parameters in this configuration, see *Liu and Pasko* [2006]. The simulation domain is discretized over 1001×241 regular grid points with the spatial resolution defined by $\Delta z = 8\times10^{-6}\times\frac{N_0}{N}$ m and $\Delta r = 8\times10^{-6}\times\frac{N_0}{N}$ m.

2.2. Optical Emissions Model

Along with the streamer propagation, we quantify the densities of excited species $N_2(a^1\Pi_g)$, $N_2(B^3\Pi_g)$, $N_2(C^3\Pi_u)$, and $N_2^+(B^2\Sigma_u^+)$ associated with optical emissions of the Lyman-Birge-Hopfield bands system of N_2 (LBH) ($a^1\Pi_g \rightarrow X^1\Sigma_g^+$), the first positive bands systems of N_2 ($1PN_2$) ($B^3\Pi_g \rightarrow A^3\Sigma_u^+$), the second positive bands system of N_2 ($2PN_2$) ($C^3\Pi_u \rightarrow B^3\Pi_g$), and the first negative bands systems of N_2^+ ($1NN_2^+$) ($B^2\Sigma_u^+ \rightarrow X^2\Sigma_g^+$), respectively. As reported in the study by *Liu and Pasko* [2005], we consider that $N_2(a^1\Pi_g)$ is quenched by N_2 and O_2 with rate coefficients $\alpha_1 = 10^{-11}$ cm^3/s and $\alpha_2 = 10^{-10}$ cm^3/s, respectively. As used by *Xu et al.* [2015], the quenching of $N_2(B^3\Pi_g)$ and $N_2(C^3\Pi_u)$ is considered to occur through collisions with N_2 and O_2 with rate coefficients $\alpha_1 = 10^{-11}$ cm^3/s [*Kossyi et al.*, 1992] and $\alpha_2 = 3\times10^{-10}$ cm^3/s [*Vallance Jones*, 1974, p. 119], respectively. $N_2^+(B^2\Sigma_u^+)$ is quenched by N_2 with a rate coefficient $\alpha_1 = 4.53\times10^{-10}$ cm^3/s and by O_2 with a rate coefficient $\alpha_2 = 7.36\times10^{-10}$ cm^3/s [e.g., *Mitchell*, 1970; *Pancheshnyi et al.*, 1998; *Kuo et al.*, 2005].

The density of excited species is estimated according to the following differential equation [e.g., *Liu and Pasko*, 2004]:

$$\frac{\partial n_k}{\partial t} = -\frac{n_k}{\tau_k} + \nu_k n_e + \sum_m n_m A_m \tag{1}$$

where $\tau_k = [A_k + \alpha_1^k N_{N_2} + \alpha_2^k N_{O_2}]^{-1}$ and A_k are the characteristic lifetime and Einstein coefficient of the excited species k, respectively. The corresponding A_k [e.g., *Liu*, 2006] and quenching coefficients taken into account for $N_2(a^1\Pi_g)$, $N_2(B^3\Pi_g)$, $N_2(C^3\Pi_u)$, and $N_2^+(B^2\Sigma_u^+)$ are shown in Table 1. One considers a simple atmospheric composition of 80% of nitrogen and 20% oxygen: $N_{N_2} = 0.8\times N$ and $N_{O_2} = 0.2\times N$. The quantities n_k and ν_k are, respectively, the density and the excitation frequency of the excited species of the state k. As the streamer model is based on the local electric field approximation, the excitation frequency ν_k depends on the local electric field or equivalently on the electron energy. The sum over $n_m A_m$ takes into account the increase in n_k resulting from the cascading of excited species from higher energy levels m. In this work, we only take into account the cascading from $N_2(C^3\Pi_u)$ to $N_2(B^3\Pi_g)$.

Moreover, the associated optical emissions are evaluated in terms of photon flux according to the following integral along the line of sight [e.g., *Liu and Pasko*, 2004]:

$$I_k = 10^{-6}\int_L A_k n_k dl \tag{2}$$

where I_k and n_k are the intensity of optical emissions in rayleighs (R) (number of photons per unit surface area and per unit time ($cm^{-2}s^{-1}$)) and the number density of excited species k, respectively. In this paper, we use a simplified chemistry model taking into account reactions relevant over short timescales: ionization by electron impact, dissociative attachment, photoionization, and the excited species produced by a streamer [*Ihaddadene and Celestin*, 2015].

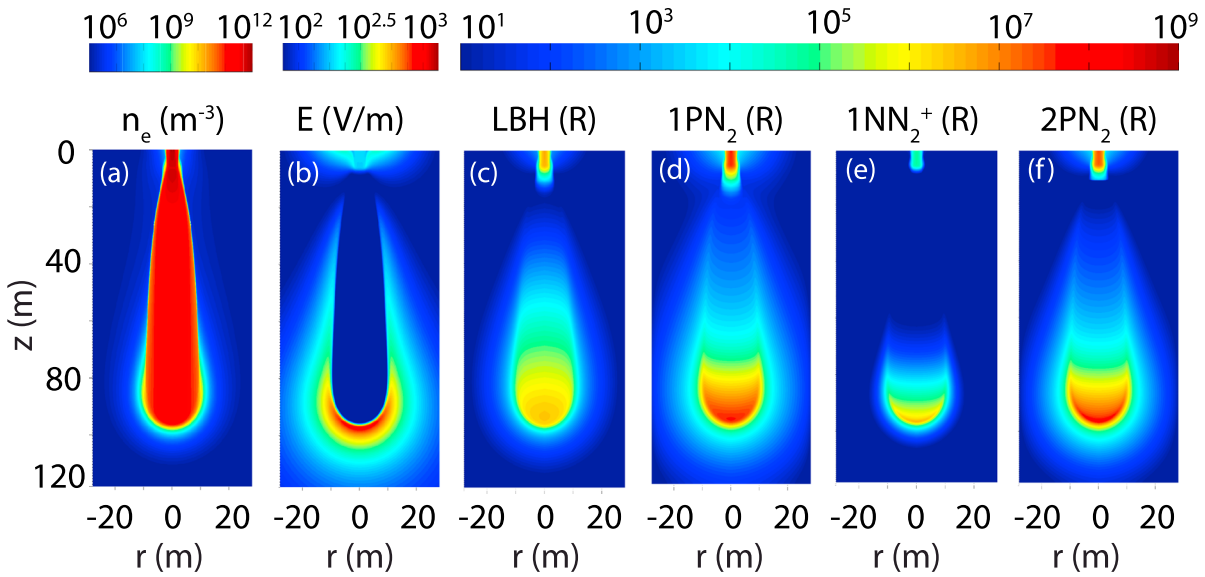


Figure 1. (a) Electron density and (b) electric field cross-sectional views. Cross-sectional views of optical emission from (c) LBH, (d) $1PN_2$, (e) $1NN_2^+$, and (f) $2PN_2$ bands systems, in units of rayleighs (R). The ambient field is $E_0 = 12 \times \frac{N}{N_0}$ kV/cm, and the altitude is $h = 70$ km.

2.3. Estimation of the Streamer Peak Electric Field Using Optical Emissions

The study of the N_2 and N_2^+ optical emissions produced by sprite streamers is useful to estimate the peak electric field in streamer heads, because the energy of the electrons depends on the amplitude of this field and the excited species responsible for the production of different bands systems are produced through collisions between electrons and N_2 molecules in the ground state and correspond to different energy thresholds. In this subsection, we describe how we proceed to infer the peak electric field.

We simulate downward propagating positive streamers in uniform electric fields $E_0 = 12\times\frac{N}{N_0}$ and $28\times\frac{N}{N_0}$ kV/cm at given altitudes h = 50, 60, 70, 80, and 90 km. Using equations (1) and (2), we quantify the excited species and the associated optical emissions (see Figure 1). The whole volume of the streamer emits photons, mainly in the head region [e.g., *Bonaventura et al.*, 2011], and hence, we integrate each band system photon flux over the whole body of the streamer including the head as $\tilde{I}_k = \int I_k \mathrm{d}s$, where $\mathrm{d}s = \Delta z \times \Delta r$ is an elementary surface. We then calculate the associated ratios $R_{kk'} = \frac{\tilde{I}_k}{\tilde{I}_{k'}}$.

Assuming that the steady state is reached (the production and loss rates of excited species are equal) under a given electric field and using equation (1) as described in *Celestin and Pasko* [2010], one obtains the following photon flux ratio, which is a function of the electric field through ν_k and $\nu_{k'}$:

$$R_{kk'} = \frac{\nu_k}{\nu_{k'}} \frac{A_k}{A_{k'}} \frac{\tau_k}{\tau_{k'}} \tag{3}$$

where we neglected the cascading from higher states. In the case of $N_2(B^3\Pi_g)$, one needs to take into account the cascading from $N_2(C^3\Pi_u)$ to $N_2(B^3\Pi_g)$ and following the same procedure, one finds

$$R_{kB^3\Pi_g} = \frac{\nu_k}{\nu_{B^3\Pi_g}} \frac{A_k}{A_{B^3\Pi_g}} \frac{\tau_k}{\tau_{B^3\Pi_g}} \frac{1}{\left(1 + \frac{\nu_{C^3\Pi_u} A_{C^3\Pi_u} \tau_{C^3\Pi_u}}{\nu_{B^3\Pi_g}}\right)} \tag{4}$$

As mentioned in *Celestin and Pasko* [2010], the steady state of excited species is not a necessary condition for equations (3) and (4) to be applicable, even though equations (3) and (4) have been derived assuming steady state. In fact, it can be shown formally from equation (1) that if the streamer propagation is sufficiently stable over a timescale on the order of τ_k, equations (3) and (4) also apply in the case of nonsteady state. Indeed, defining $N_k = \int n_k \mathrm{d}V$, equation (1) leads to

$$\frac{\partial N_k}{\partial t} = -\frac{N_k}{\tau_k} + \int \nu_k n_e \mathrm{d}V + \sum_m N_m A_m \tag{5}$$

Table 2. Correction Factors Calculated at Different Altitudes Under $E_0 = 12 \times \frac{N}{N_0}$ kV/cm Using Equations (3) and (4)

	Altitude (km)				
	50	60	70	80	90
$\frac{2PN_2}{1PN_2}$	1.57	1.60	1.68	1.62	1.64
$\frac{LBH}{1PN_2}$	2.06	2.09	2.05	2.02	1.79
$\frac{2PN_2}{1NN_2^+}$	1.40	1.41	1.40	1.41	1.41
$\frac{LBH}{1NN_2^+}$	1.36	1.36	1.38	1.38	1.41

Assuming that the streamer is sufficiently stable, i.e., its radius is approximately constant over a timescale τ_k, that is $|\frac{\partial N_k}{\partial t}| \ll \frac{N_k}{\tau_k}$, one can neglect the left-hand side of equation (5), and therefore,

$$N_k = \tau_k \int \nu_k n_e dV + \tau_k \sum_m N_m A_m \tag{6}$$

which leads to equations (3) and (4) for a given homogeneous electric field. However, although the homogeneous electric field assumption for steady state optical emissions is justified by the fact that the emission is confined in the streamer head (within a spatial shift mentioned in section 1), one might wonder whether this assumption would still be valid in the case of nonsteady state emission that trails behind the streamer head. Equation (6) can be rewritten

$$N_k = \tau_k \nu_k \int n^*_{e,\nu_k} dV + \tau_k \sum_m N_m A_m \tag{7}$$

where n^*_{e,ν_k} is an effective quantity defined by $\int \nu_k n_e dV = \nu_k \int n^*_{e,\nu_k} dV$. Since the excitation frequency strongly depends on the electric field, one can consider that $\nu_k = \nu_k(E_h)$ and one notes $N^*_{e,\nu_k} = \int n^*_{e,\nu_k} dV$. Neglecting the cascading term in equation (7), one gets

$$N_k = \tau_k \nu_k N^*_{e,\nu_k} \tag{8}$$

and thus, the ratio obtained in equation (3) if one assumes $\frac{N^*_{e,\nu_k}}{N^*_{e,\nu_{k'}}} = 1$, i.e., considering that the excitation taking place in the streamer head dominates over the excitation from other regions. It can be easily shown that equation (7) also results in equation (4) if the cascading effect is not neglected. In conclusion, the steady/nonsteady nature of optical emission does not affect the validity of the ratio found in equations (3) and (4) if the streamer can be considered as stable over a timescale τ_k and if most of the excitation is produced in the head. This point is clearly demonstrated by the simulation results of *Bonaventura et al.* [2011] for $2PN_2$ and $1NN_2^+$.

Using equations (3) and (4), one can estimate the peak electric field E_e for every simulation-based ratio $R_{kk'}$ found if steady state is reached for excited species k and k'. From the estimated field E_e and the peak field in the simulation E_h, a correction factor due mostly to the spatial shift between maxima of optical emissions and the peak electric field is calculated as $\gamma^{h,E_0}_{kk'} = \frac{E_h}{E_e}$ [*Celestin and Pasko*, 2010]. The correction factors calculated in the present work are shown in Tables 2 and 3.

However, in general, a sprite streamer can be considered as expanding exponentially in time [e.g., *N. Y. Liu et al.*, 2009]. The rate of expansion v_e is a strong function of the ambient electric field [*Kosar et al.*, 2012].

Table 3. Correction Factors Calculated at Different Altitudes Under $E_0 = 28 \times \frac{N}{N_0}$ kV/cm Using Equations (3) and (4)

	Altitude (km)				
	50	60	70	80	90
$\frac{2PN_2}{1PN_2}$	1.49	1.65	2.03	2.24	2.39
$\frac{LBH}{1PN_2}$	5.86	6.41	6.45	4.81	2.73
$\frac{2PN_2}{1NN_2^+}$	1.61	1.61	1.60	1.61	1.62
$\frac{LBH}{1NN_2^+}$	1.34	1.35	1.40	1.49	1.62

Table 4. The Expansion Frequency ν_e (s^{-1}) Calculated at Different Altitudes

	Altitude (km)				
	50	60	70	80	90
$E_0 = 12 \times \frac{N}{N_0}$ kV/cm	1.2×10^5	3.5×10^4	1.0×10^4	2.3×10^3	3.5×10^2
$E_0 = 28 \times \frac{N}{N_0}$ kV/cm	3.96×10^5	1.2×10^5	3.4×10^4	7.75×10^3	1.2×10^3

In fact, equation (5) can be rewritten in the form

$$\frac{\partial N_k}{\partial t} = -\frac{N_k}{\tau_k} + \nu_k N^*_{e,\nu_k} + \sum_m A_m N_m \tag{9}$$

As we mentioned just above, one considers that $N_k = N_{k,0} \exp(\nu_e t)$, and equation (9) leads to

$$N_k = \frac{\nu_k \tau_k N^*_{e,\nu_k}}{(1 + \nu_e \tau_k)} \tag{10}$$

if one neglects the cascading effect, and otherwise,

$$N_k = \frac{\nu_k \tau_k}{(1 + \nu_e \tau_k)} \left(N^*_{e,\nu_k} + \frac{1}{\nu_k} \frac{\sum_m \nu_m A_m \tau_m N^*_{e,\nu_m}}{(1 + \nu_e \tau_m)} \right) \tag{11}$$

Hence, for significantly quick streamer expansion ($\nu_e \sim \frac{1}{\tau_k}$), without taking into account the cascading effect, one obtains

$$R_{kk'} = \frac{\nu_k}{\nu_{k'}} \frac{A_k}{A_{k'}} \frac{\tau_k}{\tau_{k'}} \left(\frac{1 + \nu_e \tau_{k'}}{1 + \nu_e \tau_k} \right) \frac{N^*_{e,\nu_k}}{N^*_{e,\nu_{k'}}} \tag{12}$$

and taking into account the cascading effect

$$R_{kB^3\Pi_g} = \frac{\nu_k}{\nu_{B^3\Pi_g}} \frac{A_k}{A_{B^3\Pi_g}} \frac{\tau_k}{\tau_{B^3\Pi_g}} \frac{\left(\frac{1+\nu_e \tau_{B^3\Pi_g}}{1+\nu_e \tau_k} \right)}{\left[\frac{N^*_{e,\nu_{B^3\Pi_g}}}{N^*_{e,\nu_k}} + \frac{\nu_{C^3\Pi_u} A_{C^3\Pi_u} \tau_{C^3\Pi_u}}{\nu_{B^3\Pi_g} \left(1+\nu_e \tau_{C^3\Pi_u} \frac{N^*_{e,\nu_{C^3\Pi_u}}}{N^*_{e,\nu_k}} \right)} \right]} \tag{13}$$

For all the cases used in the present work, we have verified that the population of $N_2(C^3\Pi_u)$ is in steady state and $\nu_e \tau_{C^3\Pi_u} \ll 1$. The excitation frequencies ν_k and their dependence on the electric field are computed based on *Moss et al.* [2006]. Using equations (12) and (13) and assuming $\frac{N^*_{e,\nu_k}}{N^*_{e,\nu_{k'}}} = 1$, i.e, considering that the excitation taking place in the streamer head dominates over the excitation from other regions, one can estimate the peak electric field E_e for every simulation-based ratio $R_{kk'}$ found as described above even in the case of non-steady state of excited species accompanied by rapid expansion of the streamer ($\nu_e \sim \frac{1}{\tau_k}$). Precisely, because in reality the ratios $\frac{N^*_{e,\nu_k}}{N^*_{e,\nu_{k'}}} \neq 1$, correction factors need to be quantified using modeling results and taken into account in photometric-based observational studies to correct the estimated value of the peak electric field. The expansion frequency ν_e and the various correction factors calculated in the present work for different altitudes and under different uniform electric fields $E_0 = 12 \times \frac{N}{N_0}$ and $28 \times \frac{N}{N_0}$ kV/cm are shown in Tables 4–6.

Table 5. Correction Factors Calculated at Different Altitudes Under $E_0 = 12 \times \frac{N}{N_0}$ kV/cm Using Equations (12) and (13)

	Altitude (km)				
	50	60	70	80	90
$\frac{2PN_2}{1PN_2}$	1.88	1.84	1.81	1.66	1.66
$\frac{LBH}{1PN_2}$	1.39	1.39	1.39	1.58	1.69
$\frac{LBH}{1NN_2^+}$	1.48	1.47	1.47	1.43	1.42

Table 6. Correction Factors Calculated at Different Altitudes Under $E_0 = 28 \times \frac{N}{N_0}$ kV/cm Using Equations (12) and (13)

	Altitude (km)				
	50	60	70	80	90
$\frac{2PN_2}{1PN_2}$	2.65	2.63	2.61	2.43	2.44
$\frac{LBH}{1PN_2}$	1.95	1.93	1.94	2.03	2.21
$\frac{LBH}{1NN_2^+}$	1.72	1.71	1.71	1.67	1.67

3. Results

3.1. Streamer Modeling

We conducted simulations at altitudes h = 50, 60, 70, 80, and 90 km under $E_0 = 12$ and $28 \times \frac{N}{N_0}$ kV/cm, which represents 10 simulations in total. All the results produced will be described in detail in subsection 3.2.

As an example, we show the results for a positive downward propagating sprite streamer in uniform electric field $E_0 = 12 \times \frac{N}{N_0}$ kV/cm, initiated at 70 km altitude in Figures 1 and 2. Figures 1a and 1b show the cross-sectional views of the electron density and the electric field. Cross-sectional views of photon fluxes from LBH, $1PN_2$, $2PN_2$, and $1NN_2^+$ bands systems at time $t = 0.27$ ms are shown in Figures 1c–1f. The quenching altitude is defined so that above this altitude, the radiative deexcitation of given N_2 or N_2^+ excited state k dominates the collisional one. Based on the quenching coefficients that we have applied to quantify the densities of N_2 and N_2^+ excited species and their associated bands systems, we have deduced the quenching altitudes shown in Table 1.

Figures 2a and 2b show the electron density and electric field profiles along the axis of the streamer every 0.054 ms. Figure 2c shows the optical emission from bands systems profiles LBH, $1PN_2$, $2PN_2$, and $1NN_2^+$, along the axis of the streamer at $t = 0.27$ ms in terms of photon flux.

3.2. Estimation of the Altitude of the Sprite Streamers Using Optical Emissions

We first define an array of electric field ranging from 0 to $600 \times \frac{N}{N_0}$ kV/cm representing actual peak electric fields in the streamer head, and then we compute the ratio associated with each value of the electric field $E_e = \frac{E_h}{\gamma_{kk'}^{h,E_0}}$. Figures 3a and 3b show two parametric representations of selected optical emission ratios through the implicit parameter E_e. The upper and lower curves that delimit shaded areas in Figure 3 correspond to background electric fields $E_0 = 12 \times \frac{N}{N_0}$ and $28 \times \frac{N}{N_0}$ kV/cm, respectively at given altitudes. Between two shaded areas the altitude is $h_1 < h < h_2$ where $h_2 - h_1 = 10$ km. For the sake of illustration, we show how the results of our simulations are located in this parametric representation (Figure 3). Red and yellow marks correspond to cases of ambient electric field amplitudes $E_0 = 12 \times \frac{N}{N_0}$ and $28 \times \frac{N}{N_0}$ kV/cm, respectively. Since the correction factors $\gamma_{kk'}^{h,E_0}$ are obtained from the same simulations, one sees that the obtained intensity ratios fall exactly on the estimated lines. One also sees that a descending streamer would take a specific path in the parametric representation illustrated in Figures 3a and 3b. This particular behavior can be used to infer physical properties of sprite streamers from photometric observations such as the electric field and mean velocity.

The mark X located by coordinates $(R_{kk'}, R_{k''k'})$ within a shaded area illustrates a situation where the peak electric field E_h would be such that $E_h^{E_0=12kV/cm} < E_h < E_h^{E_0=28kV/cm}$, where $E_h^{E_0=12kV/cm}$ and $E_h^{E_0=28kV/cm}$ are shown in Table 7.

4. Discussion

For a given ambient electric field E_0, one sees in Figure 3 that curves corresponding to different altitudes are not overlapped. This is due to the different amounts of quenching that excited states are subjected to at different altitudes. Indeed, the excited states $N_2(a^1\Pi_g)$ and $N_2(B^3\Pi_g)$, which are responsible for LBH and $1PN_2$ bands systems, respectively, have quenching altitudes of 77 km and 67 km, while $N_2(C^3\Pi_u)$ and $N_2^+(B^2\Sigma_u^+)$, which are responsible for the $2PN_2$ and $1NN_2^+$ bands systems, respectively, can be considered as not strongly affected by quenching over the altitude range covered by sprites (see Table 1). This discrimination in altitude, which exists over a large range of electric fields in the streamer head for the selected ratios in Figure 3, is of first interest to determine the altitude of sprite streamers at various moments of time from photometric measurements. It especially applies to satellite observations in a nadir-viewing geometry. It is important to note

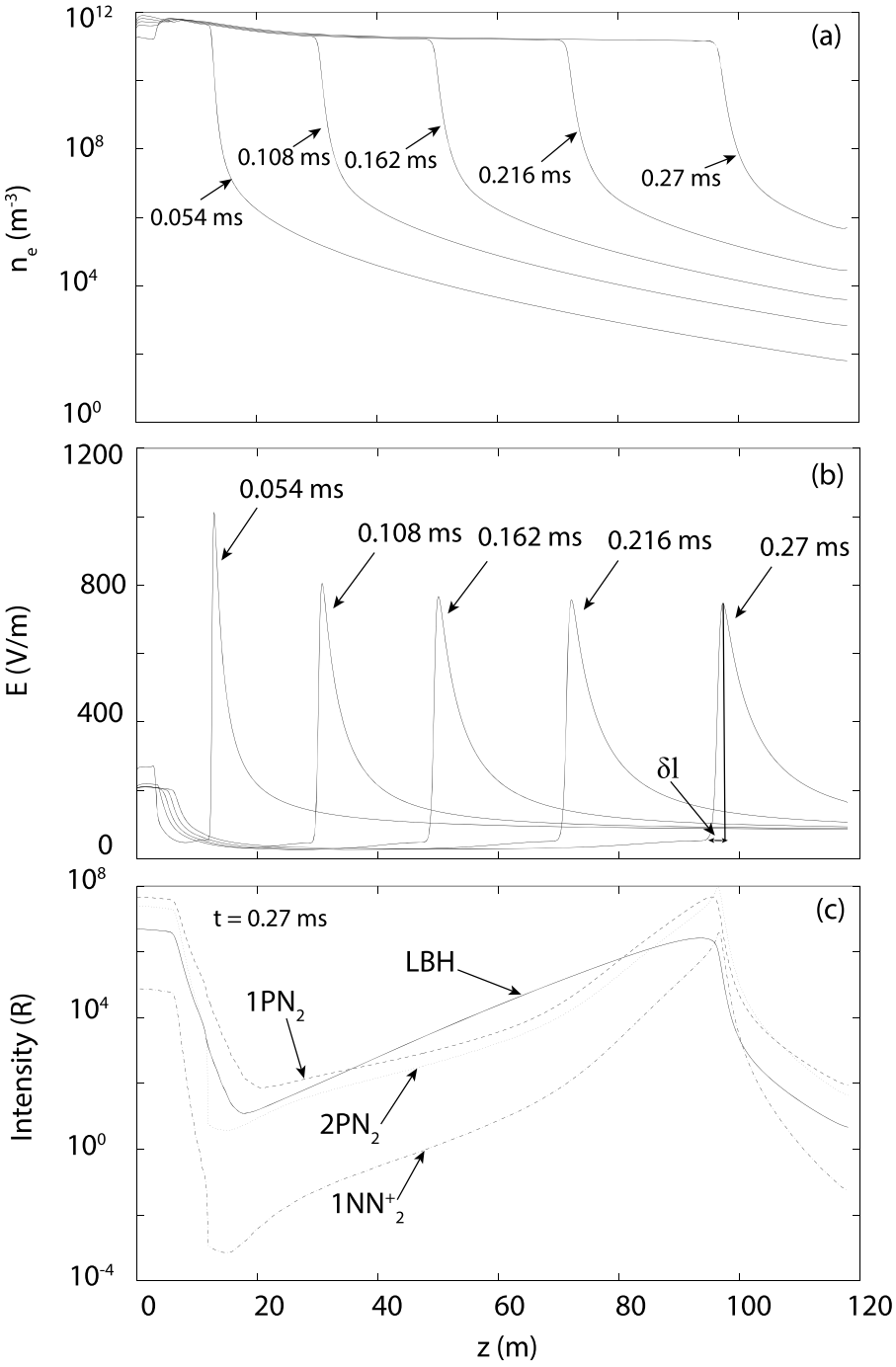


Figure 2. (a) Electron density, (b) electric field, and (c) optical emission profiles from LBH, $1PN_2$, $1NN_2^+$, and $2PN_2$ bands systems, along the axis of the streamer. The ambient field is $E_0 = 12 \times \frac{N}{N_0}$ kV/cm, and the altitude is $h = 70$ km. The quantity δl is the characteristic distance over which the gradient of the electric field is strong in the streamer head.

that the quenching coefficients for $N_2(a^1\Pi_g)$ are not well known [e.g., *Liu and Pasko*, 2005]. However, one also notes that *N. Liu et al.* [2009] obtained a satisfying agreement with observational results from the instrument ISUAL (Imager of Sprites and Upper Atmospheric Lightning) on the FORMOSAT-2 Taiwanese satellite using the quenching coefficients reported in Table 1 concerning $N_2(a^1\Pi_g)$.

At a given location, the electric field at the streamer head varies within a timescale $\delta t \sim \frac{\delta l}{V_{str}}$ (see Figure 2), where V_{str} is the streamer velocity, to be compared to the characteristic lifetime τ_k of the excited species.

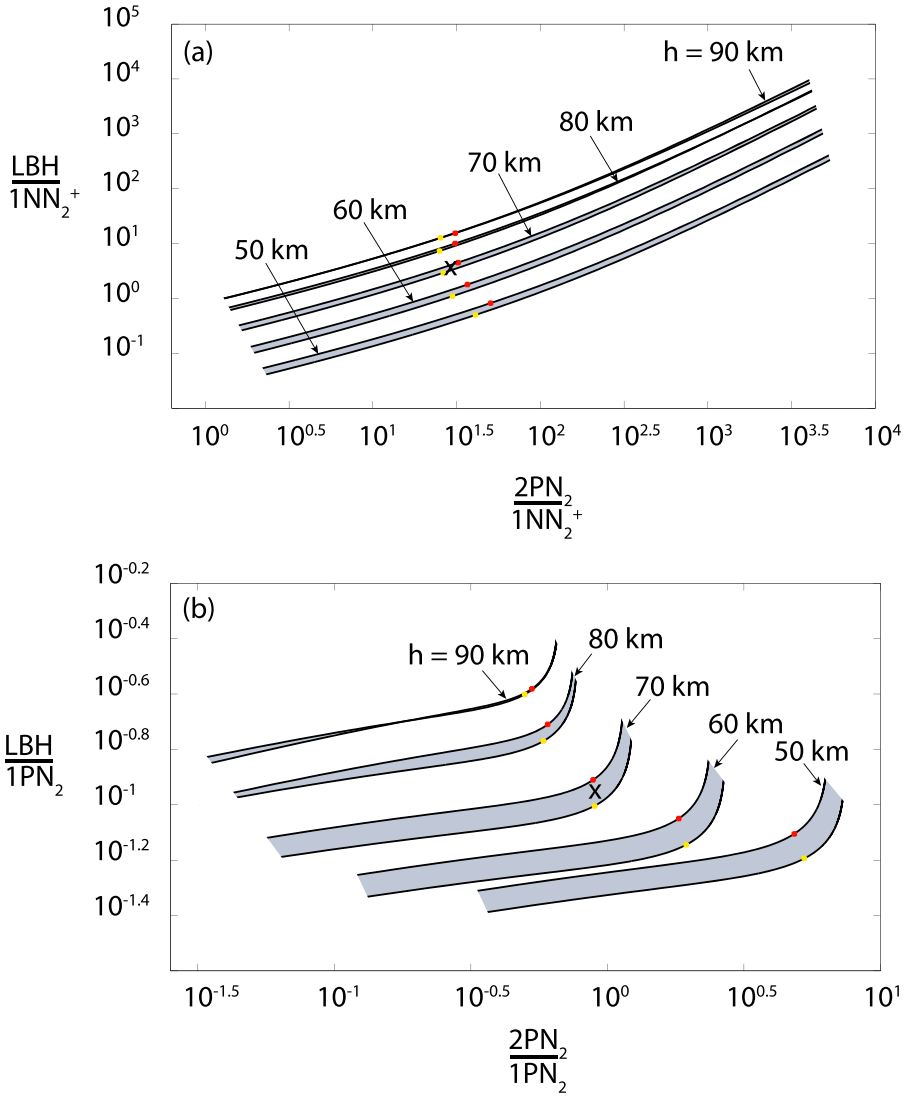


Figure 3. (a, b) Parametric representation of optical emission ratios at different altitudes. Marks in red and yellow correspond to streamer simulation results under $E_0 = 12 \times \frac{N}{N_0}$ and $28 \times \frac{N}{N_0}$ kV/cm, respectively.

From the simulations, δt is estimated to be ~5.7 and 2.5 μs at 70 km altitude under $12 \times \frac{N}{N_0}$ and $28 \times \frac{N}{N_0}$ kV/cm, respectively, while τ_k of the excited species $N_2(a^1\Pi_g)$, $N_2(B^3\Pi_g)$, $N_2(C^3\Pi_u)$, and $N_2^+(B^2\Sigma_u^+)$ are estimated to be ~14.5, 3.4, 0.049, and 0.067 μs, respectively. Therefore, one sees that the populations of $N_2(a^1\Pi_g)$ and $N_2(B^3\Pi_g)$ are not in steady state ($\tau_k > \delta t$), although $N_2(C^3\Pi_u)$ and $N_2^+(B^2\Sigma_u^+)$ are in steady state ($\tau_k < \delta t$).

Moreover, the lifetime τ_k of a given bands system does not change significantly with altitude above its corresponding quenching altitude as it is mostly defined by its Einstein coefficient A_k. Below the quenching altitude, τ_k is mostly controlled by quenching and scales as $1/N$. However, the characteristic timescale δt of

Table 7. Electric Field at the Head of the Positive Streamer E_h (V/m) at Different Altitudes Under Different Ambient Electric Fields E_0

	Altitude (km)				
	50	60	70	80	90
$E_0 = 12 \times \frac{N}{N_0}$ kV/cm	8735	2597	745.9	165.9	26.4
$E_0 = 28 \times \frac{N}{N_0}$ kV/cm	1.1×10^4	3269	940.5	209.1	33.21

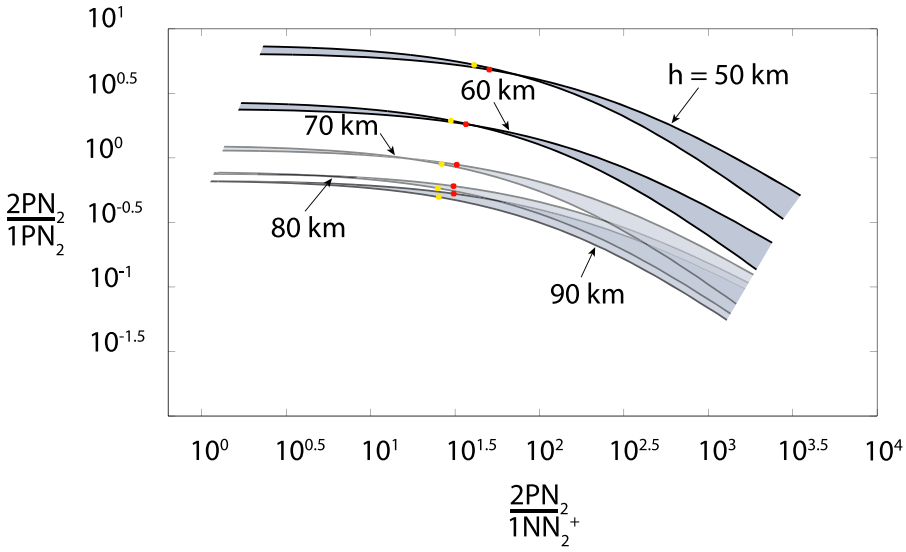


Figure 4. Parametric representation of optical emission ratios at different altitudes, to be used for comparison between satellite measurements and ground observations. Marks in red and yellow correspond to streamer simulation results under $E_0 = 12 \times \frac{N}{N_0}$ and $28 \times \frac{N}{N_0}$ kV/cm, respectively.

electric field variation in the streamer head scales as $1/N$ for all altitudes. As discussed above, the comparison between δt and τ_k determines whether the population of an excited state giving rise to a bands system is in steady state [see *Celestin and Pasko*, 2010, section 3]. Since τ_k is constant above the quenching altitude, there is an altitude above which $\delta t > \tau_k$, and hence, steady state is reached. For example, although $N_2(a^1\Pi_g)$ is not in steady state over most of the altitude range covered by sprites streamers (40–80 km), it can be considered to be in steady state at an altitude of 90 km. However, since δt scales as τ_k below the quenching altitude, the steady/nonsteady state nature of an excited species is locked below this altitude.

It is usually considered that LBH cannot be observed from the ground due to absorption in the atmosphere. However, ground observations have access to $2PN_2$, $1PN_2$, and $1NN_2^+$ bands systems (see references in the section 1). A similar parametric representation as in Figure 3 is shown in Figure 4 with these bands systems. One sees that the altitude discrimination given by parametric representation is valid only for altitudes ranging between 50 and ~70 km because of the overlap of different altitude curves that occurs above 70 km. This is an illustration of the suppression of quenching (specifically on $1PN_2$), upon which the method presented in this paper is based. As the ratio $\frac{2PN_2}{1NN_2^+}$ mostly depends on the electric field in the streamer head [e.g., *Celestin and Pasko*, 2010] and $\frac{2PN_2}{1PN_2}$ is weakly dependent on this field, the parametric representation presented in Figure 4 is well defined to measure altitude. It is interesting to note that *Garipov et al.* [2013] have used the ratio $\frac{2PN_2}{1PN_2}$ to make an estimate on the altitude of events observed by the Tatiana-2 satellite. The method we propose here is expected to be much more accurate because it is based on simulations of streamers and we take into account the corrected streamer electric field.

Table 8. Estimated Ratio $\frac{N^*_{e,v_k}}{N^*_{e,v_{k'}}}$ Under $E_0 = 12 \times \frac{N}{N_0}$ kV/cm, at Different Altitudes

	Altitude (km)				
Ratio	50	60	70	80	90
$\frac{2PN_2}{1PN_2}$	0.70	0.71	0.70	0.71	0.70
$\frac{LBH}{1PN_2}$	0.72	0.72	0.72	0.72	0.72
$\frac{2PN_2}{1NN_2^+}$	2.06	2.05	2.05	2.04	2.06
$\frac{LBH}{1NN_2^+}$	2.10	2.10	2.10	2.09	2.11

Table 9. Estimated Ratio $\frac{N^*_{e,\nu_k}}{N^*_{e,\nu_{k'}}}$ Under $E_0 = 28 \times \frac{N}{N_0}$ kV/cm, at Different Altitudes

	Altitude (km)				
Ratio	50	60	70	80	90
$\frac{2PN_2}{1PN_2}$	0.58	0.57	0.57	0.57	0.57
$\frac{LBH}{1PN_2}$	0.59	0.59	0.59	0.59	0.59
$\frac{2PN_2}{1NN_2^+}$	2.72	2.65	2.66	2.63	2.66
$\frac{LBH}{1NN_2^+}$	2.76	2.75	2.75	2.72	2.76

It is also interesting to note that the assumption $\frac{N^*_{e,\nu_k}}{N^*_{e,\nu_{k'}}} = 1$ is not necessary. In fact, one could keep this quantity in the functional dependence of the optical emission ratios (equations (12) and (13)). In this case, the correction factors become close to 1. The development of the corresponding field measurements method and its accuracy with respect to that use in the present paper is beyond the focus of the present work. However, for the sake of completeness, we have tabulated the ratios $\frac{N^*_{e,\nu_k}}{N^*_{e,\nu_{k'}}}$, for the cases studied in this paper in Tables 8 and 9. As shown in Tables 8 and 9, the ratio $\frac{N^*_{e,\nu_k}}{N^*_{e,\nu_{k'}}}$ varies between 0.57 and 2.76 in the cases studied in this paper. As explained in section 2.3, correction factors are introduced to compensate the error on the estimated peak field involved by the assumption that $\frac{N^*_{e,\nu_k}}{N^*_{e,\nu_{k'}}} = 1$.

Figures 3a and 3b show a gap between the curves corresponding to given altitudes under $E_0 = 12 \times \frac{N}{N_0}$ and $28 \times \frac{N}{N_0}$ kV/cm, which is larger at 50 km than at 90 km altitude. The gap is caused by the difference between the correction factors calculated under $E_0 = 12 \times \frac{N}{N_0}$ and $28 \times \frac{N}{N_0}$ kV/cm and the significance of the product $\nu_e \tau_k$ compared to unity (see equations (12) and (13)) under either one of these ambient fields. The curves tend to overlap at higher altitudes because the correction factors in both cases are getting closer. Under $E_0 = 12 \times \frac{N}{N_0}$ kV/cm the relative contribution of the optical emissions coming from the streamer channel to the total emission is less than that coming from the streamer channel propagating under $E_0 = 28 \times \frac{N}{N_0}$ kV/cm. The reason is twofold: on the one hand, the electric field in the streamer channel is relatively more intense in the $E_0 = 28 \times \frac{N}{N_0}$ kV/cm case which affects the correction factors, and on the other hand, the LBH and $1PN_2$ bands systems are not in a steady state below ~77 and 67 km, respectively. The latter effect plays a role in increasing the emission in the streamer channel more significantly under $E_0 = 28 \times \frac{N}{N_0}$ kV/cm than under $12 \times \frac{N}{N_0}$ kV/cm. Indeed, the emission in the channel is a contribution of both the streamer head that moves rapidly under $E_0 = 28 \times \frac{N}{N_0}$ kV/cm and the streamer channel itself. In contrast, when the steady state is reached, for example, for the $2PN_2$ and $1NN_2^+$ bands systems, the emission profile in the streamer only depends on the local electric field and the electron density at the given time (see Figure 2c).

Figures 3 and 4 of the present study are established based on equations (12) and (13). These equations are valid for both steady and nonsteady states, and they take into account the exponential expansion of the streamer. Considering the exponential expansion of streamers with a characteristic timescale $\tau_e = \frac{1}{\nu_e}$, one can see that if $\tau_k \ll \tau_e$, equations (12) and (13) tend to equations (3) and (4) obtained assuming that steady state is reached. This condition is fulfilled only in case of streamers propagating in weak electric field $E_0 \lesssim 10$ kV/cm (high τ_e). The exponential expansion of streamers particularly needs to be taken into account at altitudes lower than 80 km and under high background electric fields for the case of ratios composed of LBH and $1PN_2$ bands systems. However, the steady state assumption remains valid for the ratio $\frac{2PN_2}{1NN_2^+}$. The quantities ν_e and τ_e define the characteristic frequency and characteristic time of the streamer expansion, respectively. Within the time τ_e one can consider that the streamer moves within a distance proportional to the streamer radius βr_s and thus,

$$\nu_e \simeq \frac{V_{str}}{\beta r_s} \simeq \frac{\delta l \nu_h}{\beta \alpha r_s} \simeq \frac{\nu_h}{\beta \alpha^2} \tag{14}$$

Table 10. Estimated Maximum Uncertainties (%) on Different Ratios to Discriminate Between Different Altitudes Within 10 km

	Altitude (km)			
	50–60	60–70	70–80	80–90
$\frac{2PN_2}{1PN_2}$	46	36.82	21.21	7.87
$\frac{LBH}{1PN_2}$	5.69	15.94	26.46	19
$\frac{2PN_2}{1NN_2^+}$	15.72	6.27	2.55	0.635
$\frac{LBH}{1NN_2^+}$	37.72	44.96	43.12	27.14

See Figure 2 for an illustration of the characteristic length $\delta l \sim \frac{r_s}{\alpha}$ [e.g., *D'yakonov and Kachorovskii*, 1989]. $V_{str} = \frac{\delta l \nu_h}{\alpha}$ is the streamer velocity, and $\alpha = \ln(\frac{n_{e_c}}{n_{e_0}})$ [e.g., *Kulikovsky*, 1997; *Babaeva and Naidis*, 1997], where n_{e_c} is the electron density in the streamer channel and n_{e_0} is the electron density taken at a distance r_s from the position of the peak electric field. In the present study, we have $\alpha \sim 13$. The quantity ν_h is the ionization frequency in the streamer head. We estimate β using ν_e obtained in the simulations and equation (14) and found it to be between ~1.4 and 2.4 under $E_0 = 12 \times \frac{N}{N_0}$ and $28 \times \frac{N}{N_0}$ kV/cm, respectively. Based on the simulation and equations (10) and (11), the exponential expansion of the number of excited molecules N_k is caused by the exponential expansion of N^*_{e,ν_k}, which is related to the exponential expansion of the radius r_s of the streamer and hence the volume of the streamer head region.

Moreover, the integration of the optical emissions chosen in this work does not take into account the nonphysical contribution to the optical emissions produced in the region near the sphere electrode used in our simulations, where the electric field is strong enough (~3 E_k) to generate excited species. However, we have included the emission from the streamer channel since it is considered to be physical [*Liu*, 2010].

We expect that the proposed method is particularly applicable in case of columniform sprite events that consist of only a few descending streamers. The altitude of positive streamers at the beginning of the developments of carrot sprites could be obtained as well. However, it is predicted that the complexity introduced by the many ascending negative streamers will prevent obtaining clear results at later moments of the carrot sprite development.

It is expected that the various optical emissions involved in the presented method will not be significantly modified by the transmission through the atmosphere. Preliminary estimates show that emissions between 200 and 240 nm produced at 50 km and observed in a nadir-viewing geometry would be reduced by only ~10% (T. Farges, personal communication, 2016). In fact, as the signal is detected by photometers on board the satellite at a known location, the effect of atmospheric transmission can be accounted for in a given geometry for the proposed method to be applicable. For an estimation of the altitude within 10 km using the approach developed in the present paper, the maximum uncertainties that are acceptable on different observed ratios have been estimated approximately under $E_0 = 28 \times \frac{N}{N_0}$ kV/cm and are indicated in Table 10. We note that more precise models of populations of excited species [e.g., see *Eastes*, 2000], along with accurate quenching coefficients, may need to be implemented to improve the accuracy of the parametric representations shown in Figures 3 and 4, and the method should be first calibrated using joint campaigns associating ground-based (which can resolve the streamers altitudes) and satellite measurements.

Because of the restrictions imposed by the model, the method developed in the present paper is based on separate local streamer simulations conducted at different altitudes under similar conditions [e.g., *Pasko*, 2006; *Qin and Pasko*, 2015] and reasonable values of the ambient electric field needed for the propagation of sprite streamers $\frac{E_0}{E_k} \sim 0.4$ and 0.9 [e.g., *Hu et al.*, 2007; *Li et al.*, 2008; *N. Y. Liu et al.*, 2009; *Qin et al.*, 2013b]. It will be very interesting to push the simulation beyond and compare with simulations of streamers initiated under more realistic conditions of ambient electric field, charges species, and ionospheric inhomogeneities [e.g., *Liu et al.*, 2015, 2016] and to study the application of the method introduced in the present paper.

Finally, we note that the method might also be used for other streamer-based TLEs like upward propagating gigantic jets [e.g., *Kuo et al.*, 2009].

5. Summary and Conclusions

The following are the findings of this study:

1. We have developed a simulation-based method to infer the altitude of propagating sprite streamers from photometric measurements.
2. The method can also be used to estimate the electric field E_h at the head of propagating sprite streamers and to give information about their velocities.
3. We have estimated analytically the photon flux ratios under a nonsteady state assumption of optical emissions taking into account the exponential growth of sprite streamers.
4. We have derived a relation between the frequency ν_e associated with the expansion of the streamer and the ionization frequency ν_h at the streamer head.
5. We have calculated correction factors at different altitudes corresponding to different optical emission ratios under different background electric fields $E_0 = 12\times\frac{N}{N_0}$ and $28\times\frac{N}{N_0}$ kV/cm under steady and nonsteady state assumptions.
6. The method needs to be tested and calibrated because of its sensitivity to the excited species model and the quenching coefficients. We suggest that the verification of the method could be performed using joint observation campaigns associating ground-based and satellite measurements.
7. We suggest that a new method could be developed using simulation-driven values of the optical emission ratios ($\frac{N^*_{e,\nu_k}}{N^*_{e,\nu_{k'}}} \neq 1$). Its accuracy should be compared with the method elaborated in the present paper.
8. The method is expected to improve the scientific return of ISUAL, GLIMS, ASIM, and TARANIS space missions and ground observation campaigns.

Acknowledgments
The authors thank Thomas Farges (CEA/DAM/DIF, France) for very useful discussions in preparation of this paper. This work is supported by the French Space Agency (CNES) as part of TARANIS space mission and by the French Region Centre-Val de Loire. Some results of simulation presented in this paper have been obtained using the computer cluster at the Centre de Calcul Scientifique en Région Centre-Val de Loire (CCSC). All data used in this paper are directly available after a request is made to author M.A.I. (mohand.ihaddadene@cnrs-orleans.fr) or S.C. (sebastien.celestin@cnrs-orleans.fr).

References

Adachi, T., H. Fukunishi, Y. Takahashi, and M. Sato (2004), Roles of the EMP and QE field in the generation of columniform sprites, *Geophys. Res. Lett.*, *31*, L04107, doi:10.1029/2003GL019081.

Adachi, T., et al. (2006), Electric field transition between the diffuse and streamer regions of sprites estimated from ISUAL/array photometer measurements, *Geophys. Res. Lett.*, *33*, L17803, doi:10.1029/2006GL026495.

Armstrong, R. A., J. A. Shorter, M. J. Taylor, D. M. Suszcynsky, W. A. Lyons, and L. S. Jeong (1998), Photometric measurements in the SPRITES '95 '96 campaigns of nitrogen second positive (399.8 nm) and first negative (427.8 nm) emissions, *J. Atmos. Sol. Terr. Phys.*, *60*, 787–799, doi:10.1016/S1364-6826(98)00026-1.

Babaeva, N. Y., and G. V. Naidis (1996a), Simulation of positive streamers in air in weak uniform electric fields, *Phys. Lett. A*, *215*, 187–190, doi:10.1016/0375-9601(96)00225-3.

Babaeva, N. Y., and G. V. Naidis (1996b), Two-dimensional modelling of positive streamer dynamics in non-uniform electric fields in air, *J. Phys. D: App. Phys.*, *29*, 2423–2431, doi:10.1088/0022-3727/29/9/029.

Babaeva, N. Y., and G. V. Naidis (1997), Dynamics of positive and negative streamers in air in weak uniform electric fields, *IEEE Trans. Plasma Sci.*, *25*, 375–379, doi:10.1109/27.602514.

Blanc, E., T. Farges, R. Roche, D. Brebion, T. Hua, A. Labarthe, and V. Melnikov (2004), Nadir observations of sprites from the International Space Station, *J. Geophys. Res.*, *109*, A02306, doi:10.1029/2003JA009972.

Bonaventura, Z., A. Bourdon, S. Celestin, and V. P. Pasko (2011), Electric field determination in streamer discharges in air at atmospheric pressure, *Plasma Sources Sci. Technol.*, *20*(3), 035012, doi:10.1088/0963-0252/20/3/035012.

Bucsela, E., J. Morrill, M. Heavner, C. Siefring, S. Berg, D. Hampton, D. Moudry, E. Wescott, and D. Sentman (2003), $N_2(B^3\Pi_g)$ and $N_2^+(A^2\Pi_u)$ vibrational distributions observed in sprites, *J. Atmos. Sol. Terr. Phys.*, *65*, 583–590, doi:10.1016/S1364-6826(02)00316-4.

Celestin, S., and V. P. Pasko (2010), Effects of spatial non-uniformity of streamer discharges on spectroscopic diagnostics of peak electric fields in transient luminous events, *Geophys. Res. Lett.*, *37*, L07804, doi:10.1029/2010GL042675.

Chen, A. B., et al. (2008), Global distributions and occurrence rates of transient luminous events, *J. Geophys. Res.*, *113*, A08306, doi:10.1029/2008JA013101.

Committee on Extension to the Standard Atmosphere (1976), *U.S. Committee on Extension to the Standard Atmosphere; U.S. Standard Atmosphere, 1976*, U.S. Government Printing Office, Washington, D. C.

D'yakonov, M. I., and V. Y. Kachorovskii (1989), Streamer discharge in a homogeneous field, *Zh. Eksp. Teor. Fiz.*, *95*(5), 1850–1859.

Eastes, R. W. (2000), Modeling the N_2 Lyman-Birge-Hopfield bands in the dayglow: Including radiative and collisional cascading between the singlet states, *J. Geophys. Res.*, *105*(A8), 18,557–18573, doi:10.1029/1999JA000378.

Franz, R. C., R. J. Nemzek, and J. R. Winckler (1990), Television image of a large upward electrical discharge above a thunderstorm system, *Science*, *249*, 48–51, doi:10.1126/science.249.4964.48.

Garipov, G. K., et al. (2013), Global transients in ultraviolet and red-infrared ranges from data of Universitetsky-Tatiana-2 satellite, *J. Geophys. Res. Atmos.*, *118*, 370–379, doi:10.1029/2012JD017501.

Gerken, E. A., U. S. Inan, and C. P. Barrington-Leigh (2000), Telescopic imaging of sprites, *Geophys. Res. Lett.*, *27*, 2637–2640, doi:10.1029/2000GL000035.

Gordillo-Vázquez, F. J. (2010), Vibrational kinetics of air plasmas induced by sprites, *J. Geophys. Res.*, *115*, A00E25, doi:10.1029/2009JA014688.

Gordillo-Vázquez, F. J., A. Luque, and M. Simek (2011), Spectrum of sprite halos, *J. Geophys. Res.*, *116*, A09319, doi:10.1029/2011JA016652.

Gordillo-Vázquez, F. J., A. Luque, and M. Simek (2012), Near infrared and ultraviolet spectra of TLEs, *J. Geophys. Res.*, *117*, A05329, doi:10.1029/2012JA017516.

Green, B. D., et al. (1996), Molecular excitation in sprites, *Geophys. Res. Lett.*, *23*, 2161–2164, doi:10.1029/96GL02071.

Hampton, D. L., M. J. Heavner, E. M. Wescott, and D. D. Sentman (1996), Optical spectral characteristics of sprites, *Geophys. Res. Lett.*, *23*, 89–92, doi:10.1029/95GL03587.

Heavner, M. J., J. S. Morrill, C. Siefring, D. D. Sentman, D. R. Moudry, E. M. Wescott, and E. J. Bucsela (2010), Near-ultraviolet and blue spectral observations of sprites in the 320–460 nm region: N_2 (2PG) emissions, *J. Geophys. Res.*, *115*, A00E44, doi:10.1029/2009JA014858.

Hu, W., S. A. Cummer, and W. A. Lyons (2007), Testing sprite initiation theory using lightning measurements and modeled electromagnetic fields, *J. Geophys. Res.*, *112*, D13115, doi:10.1029/2006JD007939.

Ihaddadene, M. A., and S. Celestin (2015), Increase of the electric field in head-on collisions between negative and positive streamers, *Geophys. Res. Lett.*, *42*, 5644–5651, doi:10.1002/2015GL064623.

Kanmae, T., H. C. Stenbaek-Nielsen, and M. G. McHarg (2007), Altitude resolved sprite spectra with 3 ms temporal resolution, *Geophys. Res. Lett.*, *34*, L07810, doi:10.1029/2006GL028608.

Kanmae, T., H. C. Stenbaek-Nielsen, M. G. McHarg, and R. K. Haaland (2010a), Observation of blue sprite spectra at 10,000 fps, *Geophys. Res. Lett.*, *37*, L13808, doi:10.1029/2010GL043739.

Kanmae, T., H. C. Stenbaek-Nielsen, M. G. McHarg, and R. K. Haaland (2010b), Observation of sprite streamer head's spectra at 10,000 fps, *J. Geophys. Res.*, *115*, A00E48, doi:10.1029/2009JA014546.

Kosar, B. C., N. Liu, and H. K. Rassoul (2012), Luminosity and propagation characteristics of sprite streamers initiated from small ionospheric disturbances at subbreakdown conditions, *J. Geophys. Res.*, *117*, A08328, doi:10.1029/2012JA017632.

Kossyi, I. A., A. Y. Kostinsky, A. A. Matveyev, and V. P. Silakov (1992), Kinetic scheme of the non-equilibrium discharge in nitrogen-oxygen mixtures, *Plasma Sources Sci. Technol.*, *1*, 207–220, doi:10.1088/0963-0252/1/3/011.

Kulikovsky, A. A. (1997), Positive streamer between parallel plate electrodes in atmospheric pressure air, *J. Phys. D: Appl. Phys.*, *30*, 441–450, doi:10.1088/0022-3727/30/3/017.

Kuo, C.-L., R. R. Hsu, A. B. Chen, H. T. Su, L. C. Lee, S. B. Mende, H. U. Frey, H. Fukunishi, and Y. Takahashi (2005), Electric fields and electron energies inferred from the ISUAL recorded sprites, *Geophys. Res. Lett.*, *32*, L19103, doi:10.1029/2005GL023389.

Kuo, C.-L., et al. (2009), Discharge processes, electric field, and electron energy in ISUAL-recorded gigantic jets, *J. Geophys. Res.*, *114*, A04314, doi:10.1029/2008JA013791.

Lefeuvre, F., E. Blanc, J.-L. Pinçon, R. Roussel-Dupré, D. Lawrence, J.-A. Sauvaud, J.-L. Rauch, H. de Feraudy, and D. Lagoutte (2008), TARANIS A satellite project dedicated to the physics of TLEs and TGFs, *Space Sci. Rev.*, *137*, 301–315, doi:10.1007/s11214-008-9414-4.

Li, J., S. A. Cummer, W. A. Lyons, and T. E. Nelson (2008), Coordinated analysis of delayed sprites with high-speed images and remote electromagnetic fields, *J. Geophys. Res.*, *113*, D20206, doi:10.1029/2008JD010008.

Liu, N. (2006), Dynamics of positive and negative streamers in sprites, PhD thesis, Pennsylvania State Univ.

Liu, N. (2010), Model of sprite luminous trail caused by increasing streamer current, *Geophy. Res. Lett.*, *37*, L04102, doi:10.1029/2009GL042214.

Liu, N., and V. P. Pasko (2004), Effects of photoionization on propagation and branching of positive and negative streamers in sprites, *J. Geophy. Res.*, *109*, A04301, doi:10.1029/2003JA010064.

Liu, N., and V. P. Pasko (2005), Molecular nitrogen LBH band system far-UV emissions of sprite streamers, *Geophys. Res. Lett.*, *32*, L05104, doi:10.1029/2004GL022001.

Liu, N., and V. P. Pasko (2006), Effects of photoionization on similarity properties of streamers at various pressures in air, *J. Phys. D: Appl. Phys.*, *39*, 327–334, doi:10.1088/0022-3727/39/2/013.

Liu, N., et al. (2006), Comparison of results from sprite streamer modeling with spectrophotometric measurements by ISUAL instrument on FORMOSAT-2 satellite, *Geophys. Res. Lett.*, *33*, L01101, doi:10.1029/2005GL024243.

Liu, N., V. P. Pasko, H. U. Frey, S. B. Mende, H.-T. Su, A. B. Chen, R.-R. Hsu, and L.-C. Lee (2009), Assessment of sprite initiating electric fields and quenching altitude of $a^1\Pi_g$ state of N_2 using sprite streamer modeling and ISUAL spectrophotometric measurements, *J. Geophys. Res.*, *114*, A00E02, doi:10.1029/2008JA013735.

Liu, N., J. R. Dwyer, H. C. Stenbaek-Nielsen, and M. G. McHarg (2015), Sprite streamer initiation from natural mesospheric structures, *Nat. Commun.*, *6*, 7540, doi:10.1038/ncomms8540.

Liu, N., L. D. Boggs, and S. A. Cummer (2016), Observation-constrained modeling of the ionospheric impact of negative sprites, *Geophys. Res. Lett.*, *43*, 2365–2373, doi:10.1002/2016GL068256.

Liu, N. Y., V. P. Pasko, K. Adams, H. C. Stenbaek-Nielsen, and M. G. McHarg (2009), Comparison of acceleration, expansion, and brightness of sprite streamers obtained from modeling and high-speed video observations, *J. Geophys. Res.*, *114*, A00E03, doi:10.1029/2008JA013720.

Mende, S. B., R. L. Rairden, G. R. Swenson, and W. A. Lyons (1995), Sprite spectra; N_2 1 PG band identification, *Geophys. Res. Lett.*, *22*, 2633–2636, doi:10.1029/95GL02827.

Milikh, G., J. A. Valdivia, and K. Papadopoulos (1998), Spectrum of red sprites, *J. Atmos. Sol. Terr. Phys.*, *60*, 907–915, doi:10.1016/S1364-6826(98)00032-7.

Mitchell, K. B. (1970), Fluorescence efficiencies and collisional deactivation rates for N_2 and N_2^+ bands excited by soft X rays, *J. Chem. Phys.*, *53*, 1795–1802, doi:10.1063/1.1674257.

Morrill, J., et al. (2002), Electron energy and electric field estimates in sprites derived from ionized and neutral N_2 emissions, *Geophys. Res. Lett.*, *29*, 1462, doi:10.1029/2001GL014018.

Morrill, J. S., E. J. Bucsela, V. P. Pasko, S. L. Berg, M. J. Heavner, D. R. Moudry, W. M. Benesch, E. M. Wescott, and D. D. Sentman (1998), Time resolved N_2 triplet state vibrational populations and emissions associated with red sprites, *J. Atmos. Sol. Terr. Phys.*, *60*, 811–829, doi:10.1016/S1364-6826(98)00031-5.

Morrow, R., and J. J. Lowke (1997), Streamer propagation in air, *J. Phys. D: Appl. Phys.*, *30*, 614–627, doi:10.1088/0022-3727/30/4/017.

Moss, G. D., V. P. Pasko, N. Liu, and G. Veronis (2006), Monte Carlo model for analysis of thermal runaway electrons in streamer tips in transient luminous events and streamer zones of lightning leaders, *J. Geophys. Res.*, *111*, A02307, doi:10.1029/2005JA011350.

Neubert, T. (2009), ASIM an instrument suite for the International Space Station, in *American Inst. Phys. Conf. Series*, vol. 1118, pp. 8–12, doi:10.1063/1.3137718

Pancheshnyi, S. V., S. M. Starikovskaia, and A. Y. Starikovskii (1998), Measurements of rate constants of the $N_2(C^3\Pi_u, v' = 0)$ and $N_2^+(B^2\Sigma_u^+, v' = 0)$ deactivation by N_2, O_2, H_2, CO and H_2O molecules in afterglow of the nanosecond discharge, *Chem. Phys. Lett.*, *294*, 523–527, doi:10.1016/S0009-2614(98)00879-3.

Pasko, V. P. (2006), Theoretical modeling of sprites and jets, in *Sprites, Elves and Intense Lightning Discharges, NATO Science Series II: Mathematics, Physics and Chemistry*, pp. 255–311, Spring, Dordrecht, Netherlands.

Pasko, V. P. (2007), Red sprite discharges in the atmosphere at high altitude: The molecular physics and the similarity with laboratory discharges, *Plasma Sources Sci. Technol.*, *16*, S13—S29, doi:10.1088/0963-0252/16/1/S02.

Pasko, V. P., U. S. Inan, and T. F. Bell (1998), Spatial structure of sprites, *Geophys. Res. Lett.*, *25*, 2123–2126, doi:10.1029/98GL01242.

Pasko, V. P., Y. Yair, and C.-L. Kuo (2012), Lightning related transient luminous events at high altitude in the Earth's atmosphere: Phenomenology, mechanisms and effects, *Space. Sci. Rev.*, *168*, 475–516, doi:10.1007/s11214-011-9813-9.

Pasko, V. P., J. Qin, and S. Celestin (2013), Toward better understanding of sprite streamers: Initiation, morphology, and polarity asymmetry, *Surv. Geophys.*, *34*, 797–830, doi:10.1007/s10712-013-9246-y.

Qin, J., and V. P. Pasko (2014), On the propagation of streamers in electrical discharges, *J. Phys. D: Appl. Phys.*, *47*(435202), doi:10.1088/0022-3727/47/43/435202.

Qin, J., and V. P. Pasko (2015), Dynamics of sprite streamers in varying air density, *Geophys. Res. Lett.*, *42*, 2031–2036, doi:10.1002/2015GL063269.

Qin, J., S. Celestin, and V. P. Pasko (2012), Low frequency electromagnetic radiation from sprite streamers, *Geophys. Res. Lett.*, *39*, L22803, doi:10.1029/2012GL053991.

Qin, J., S. Celestin, V. P. Pasko, S. A. Cummer, M. G. McHarg, and H. C. Stenbaek-Nielsen (2013a), Mechanism of column and carrot sprites derived from optical and radio observations, *Geophys. Res. Lett.*, *40*, 4777–4782, doi:10.1002/grl.50910.

Qin, J., S. Celestin, and V. P. Pasko (2013b), Dependence of positive and negative sprite morphology on lightning characteristics and upper atmospheric ambient conditions, *J. Geophys. Res. Space Physics*, *118*, 2623–2638, doi:10.1029/2012JA017908.

Qin, J., V. P. Pasko, M. G. McHarg, and H. C. Stenbaek-Nielsen (2014), Plasma irregularities in the *D*-region ionosphere in association with sprite streamer initiation, *Nat. Commun.*, *5*, 3740, doi:10.1038/ncomms4740.

Sato, M. et al. (2015), Overview and early results of the global lightning and sprite measurements mission, *J. Geophys. Res. Atmos.*, *120*(9), 3822–3851, doi:10.1002/2014JD022428.

Siefring, C. L., J. S. Morrill, D. D. Sentman, and M. J. Heavner (2010), Simultaneous near-infrared and visible observations of sprites and acoustic-gravity waves during the EXL98 campaign, *J. Geophys. Res.*, *115*, A00E57, doi:10.1029/2009JA014862.

Stanley, M., P. Krehbiel, M. Brook, C. Moore, W. Rison, and B. Abrahams (1999), High speed video of initial sprite development, *Geophys. Res. Lett.*, *26*, 3201–3204, doi:10.1029/1999GL010673.

Stenbaek-Nielsen, H. C., D. R. Moudry, E. M. Wescott, D. D. Sentman, and F. T. S. Sabbas (2000), Sprites and possible mesospheric effects, *Geophys. Res. Lett.*, *27*, 3829–3832, doi:10.1029/2000GL003827.

Stenbaek-Nielsen, H. C., T. Kanmae, M. G. McHarg, and R. Haaland (2013), High-speed observations of sprite streamers, *Surv. Geophys.*, *34*, 769–795, doi:10.1007/s10712-013-9224-4.

Suszcynsky, D. M., R. Roussel-Dupré, W. A. Lyons, and R. A. Armstrong (1998), Blue-light imagery and photometry of sprites, *J. Atmos. Sol. Terr. Phys.*, *60*, 801–809, doi:10.1016/S1364-6826(98)00027-3.

Vallance Jones, A. V. (1974), *Aurora*, D. Reidel, Norwell, Mass.

Wescott, E. M., D. D. Sentman, M. J. Heavner, D. L. Hampton, W. A. Lyons, and T. Nelson (1998), Observations of 'Columniform' sprites, *J. Atmos. Sol. Terr. Phys.*, *60*, 733–740, doi:10.1016/S1364-6826(98)00029-7.

Winckler, J. R., R. C. Franz, and R. J. Nemzek (1993), Fast low-level light pulses from the night sky observed with the SKYFLASH program, *J. Geophys. Res.*, *98*, 8775–8783, doi:10.1029/93JD00198.

Xu, W., S. Celestin, and V. P. Pasko (2015), Optical emissions associated with terrestrial gamma ray flashes, *J. Geophys. Res. Space Physics*, *120*, 1355–1370, doi:10.1002/2014JA020425.